General Disclaimer

One or more of the Following Statements may affect this Document

- This document has been reproduced from the best copy furnished by the organizational source. It is being released in the interest of making available as much information as possible.

- This document may contain data, which exceeds the sheet parameters. It was furnished in this condition by the organizational source and is the best copy available.

- This document may contain tone-on-tone or color graphs, charts and/or pictures, which have been reproduced in black and white.

- This document is paginated as submitted by the original source.

- Portions of this document are not fully legible due to the historical nature of some of the material. However, it is the best reproduction available from the original submission.

Produced by the NASA Center for Aerospace Information (CASI)

X-692-73-322
PREPRINT

NASA TM X- 70499

A CORRELATIVE STUDY OF SSC'S, INTERPLANETARY SHOCKS, AND SOLAR ACTIVITY

(NASA-TM-X-70499) A CORRELATIVE STUDY OF SSC'S, INTERPLANETARY SHOCKS, AND SOLAR ACTIVITY (NASA) 42 p HC $4.25 CSCL 03B

N74-10755

Unclas
G3/29 21566

J. K. CHAO
R. P. LEPPING

OCTOBER 1973

GSFC
GODDARD SPACE FLIGHT CENTER
GREENBELT, MARYLAND

A Correlative Study of SSC's, Interplanetary Shocks, and Solar Activity

J. K. Chao* and R. P. Lepping
Laboratory for Extraterrestrial Physics
NASA-Goddard Space Flight Center
Greenbelt, Maryland 20771

An Extended Version of a Talk Presented at the

CONFERENCE ON FLARE-PRODUCED SHOCK WAVES IN THE CORONA AND INTERPLANETARY SPACE

(September 11-14, 1972)

High Altitude Observatory
National Center for Atmospheric Research
Boulder, Colorado 80302

September 1973

Short Title: IP Shock Correlation Study

*NAS/NRC Postdoctoral Research Associate, Now at Lunar and Planetary Laboratory, The University of Arizona, Tucson, Arizona 85721

ABSTRACT

We have examined 93 SSC's during the four year period from 1968 to 1971 at and near the peak of the solar activity cycle. Of the 93 SSC's 81 could be associated with solar activity, such as solar flares and radio bursts of Type II and Type IV. The mean propagation speeds of these flare-associated events ranged from 400 to 1000 km/sec with an average speed of 600-700 km/sec. Disturbances associated with 48 of the SSC's have been studied in detail using the corresponding interplanetary (IP) magnetic field, and plasma data when they were available. We found that 41 of the 48 disturbances corresponded to IP shock waves, and the remaining seven events were tangential discontinuities. Thirty percent of the IP shocks had thick structure (i.e. the magnetic field jump across the shock occurred over a distance much greater than 50 proton Larmor radii). Also given is a statistical study of the gross geometry of a "typical" or average shock surface based on multiple spacecraft sightings and their relative orientation with respect to the solar flare and/or solar activity. By considering the orientations of 22 well-determined shock normals in relation to the positions of the parent flares on the solar disk, which is a modification of a method given by Taylor (1969), it is suggested that a typical shock front propagating out from the sun at 1 AU has a radius of curvature on the order of 1 AU. Also given are some general properties of oblique IP flare-shocks.

Introduction

It is generally believed that most IP shock waves originate at or near the sun, in particular from a solar active region (Gold, 1955; Hirshberg, 1968; Hirshberg et al., 1970; Hundhausen, 1970; and Hundhausen et al., 1970). Some theoretical models of the propagation of flare-associated shock waves in an ambient solar wind based on similarity solutions of the hydrodynamic equations, were developed by Parker (1961), Simon and Axford (1966), Dryer (1970), and Korbeinikov (1969). Hundhausen and Gentry (1969a,b) used numerical solutions of hydrodynamic equations to simulate the propagation of flare-associated disturbances. De Young and Hundhausen (1971) found that, even for a blast confined to a cone of half-angle equal to or less than 15°, the shock front upon reaching 1 AU becomes quasi-spherical centered at approximately 0.5 AU. For a model of flare-associated IP shocks, shocks are expected to form in the vicinity of the sun and propagate outward with a shock thickness on the order of a few proton Larmor radii during most of their passage through IP space. Spherical symmetry of the shock surface may be disturbed due to IP inhomogeneities (Heinemann and Siscoe, 1973) or abrupt discontinuities (Lepping and Burlaga, 1973).

Hirshberg (1968) derived an average shape of an IP shock front from a statistical study of the magnitudes of SSC's. She concluded that flare ejected plasma is emitted on a broad front but with considerable departure from heliocentric spherical symmetry. Taylor (1969), utilizing IMP 3 observations, found that the shock front at 1 AU can be well approximated by a spherical surface whose curvature is $\simeq$ 0.75 AU and centered at $\simeq$ 0.5 AU.

In this paper we present an observational study of 38 flare-associated shocks. The shock speeds and normals have been computed accurately for 22 of these cases through the use of multiple spacecraft (S/C) observations; the speeds and normals for the remaining 16 shocks are also obtained.

The Experiments

IP data have been collected from eight S/C (Explorers 33, 34, 35, 41, 43, Pioneers 7 and 8, and OGO 5), which, taken together, cover the four year period of interest (1968 through 1971). We are primarily dealing with IP magnetic field data and the positions of pertinent S/C during the time of onset of the events. Only in a few cases were the detailed IP plasma data available to us; we used them mainly to check results obtained from the multiple S/C method and to obtain local plasma bulk speeds. Table 1 shows the S/C and the associated principal investigators for the experiments from which we obtained this data. Many of the events have been observed by more than one S/C. However, in some intervals only the magnetic field data were available. Hence, only a limited study could be made for those periods.

The Method of Study

Sudden commencements (SSC's) identified by 20 or more magnetic observatories were selected for the years 1968 to 1971 inclusive. Then for a given event the IP magnetic field data from the experiments on the S/C listed in Table 1 were examined. For the events for which the IP data were available the associated discontinuities in the magnetic field were selected. When the events had been observed by more than one S/C,

Table 1

Interplanetary Data Source

Spacecraft	Principal Investigators	
	Magnetic Field Experiements	Plasma Experiments
Explorer 33	N. F. Ness, GSFC	H. Bridge, M. I. T.
" 35	"	"
" 34	"	K. W. Ogilvie, GSFC
" 41	"	----------
" 43	"	S. J. Bame, Los Alamos and K. W. Ogilvie, GSFC
Pioneer 7	"	----------
" 8	N. F. Ness and F. Mariani, Rome	----------
OGO 5	P. J. Coleman, UCLA	----------
Explorer 33	C. P. Sonett, Ames	----------
Explorer 35	"	----------

multiple S/C methods could be used to find the normal and speed of these discontinuities. In order to find an accurate normal and speed for a given event, we used the following procedure:

First, the magnetic field data were selected for each event. The average values and their standard deviations were computed for both sides of each discontinuity (here discontinuity means shock or tangential discontinuity). The time intervals over which the averages were taken depended on the behavior of the fluctuations of the vector quantity $\vec{B}$ in the vicinity of the discontinuity. Time intervals were chosen over which this quantity displayed relatively steady behavior; these were in general 3 to 5 min long. Then, the shock normal $\hat{n}_s$ was computed for each S/C observation using the magnetic coplanarity theorem (Colburn and Sonett, 1966). The uncertainty of $\hat{n}_s$ is closely related to the fluctuations of the magnetic field in the analysis interval. However, for most IP events the computed $\hat{n}_s$'s have an uncertainty within $\approx 20°$. If the discontinuity was a tangential one, the normal to the discontinuity plane should be in the direction $\hat{n}_t$ where $\hat{n}_t = \dfrac{\vec{B}_1 \times \vec{B}_2}{|(\vec{B} \times \vec{B}_2)|}$. The direction $\hat{n}_t$ was also computed for each observation, where $\vec{B}_1$ and $\vec{B}_2$ are the average magnetic field before and after the discontinuity, respectively. The comments above concerning the expected error in $\hat{n}_s$ hold for $\hat{n}_t$; however, in general the error in $\hat{n}_t$ should be smaller, since $(\vec{B}_2 - \vec{B}_1)$ is not involved. Then the normals $\hat{n}_s$ and $\hat{n}_t$ were computed in every case regardless of whether the actual event corresponded to a shock or tangential discontinuity, and ideally they should be at 90° with repect to each other. Since in practice $\hat{n}_s$ and $\hat{n}_t$ can be distinguished from each other with

only an error of $\gtrsim 30°$ ($=\sqrt{2}\,20°$), the ideal 90°, being a factor 3 greater, generally enables highly reliable differentiation. Choosing which of the two normals was correct is another matter and is discussed below.

Secondly, multiple S/C methods, which were also used, are now described. If there were two S/C observations available, the relative position vector of these two S/C, $\Delta\vec{R} \equiv (\vec{R}_2 - \vec{R}_1)$, is related to the propagation speed of the discontinuity, V_d, and to the time difference, Δt, between observations of the discontinuity at these two S/C in the following way:

$$\Delta\vec{R} \cdot \hat{n}_d = V_d \Delta t \qquad (1)$$

where $\vec{R}_1$ and $\vec{R}_2$ are the position vectors of the two S/C and $\hat{n}_d$ and V_d are the normal and the local speed of the discontinuity, respectively. Note that we do not yet specify the type of discontinuity, i.e., shock or tangential. This calculation is based on a geometric configuration only—and kinematic assumptions to be discussed — but is independent of specific identification. Also since the normal component of the magnetic field is continuous across any type of discontinuity, then $\Delta\vec{B}$ ($\equiv(\vec{B}_2 - \vec{B}_1)$) is parallel to the surface of the discontinuity, i.e., the condition

$$\Delta\vec{B} \cdot \hat{n}_d = 0 \qquad (2)$$

holds for any type of discontinuity. It is important to note that on a scale of the order of 0.01 AU a shock front usually remains planar and propagates at a constant speed (Ogilvie and Burlaga, 1969; Chao, 1970), and similarly for tangential discontinuities on the order of 0.002 AU

(Burlaga and Ness, 1969). In all of the computations done for this study involving more than one S/C, we have assumed in fact that the discontinuities can be approximated as planar and propagate at a constant speed within the distance of the S/C separations ($\lesssim$ 0.004 AU). However, the magnetic field can change over all scale lengths. That is, the $\Delta\vec{B}$'s are not necessarily equal to each other for the two S/C observations, even though the normals remain the same. Hence, it was often useful to provide two equations of the type Eq(2), one each for the two S/C observations. Then solving Eqs(1) and (2) together yielded V_d and $\hat{n}_d$ for the discontinuity.

If three S/C observations were available, two equations of the type Eq(1) and any one equation of the type Eq(2) were enough to determine V_d and $\hat{n}_d$. In the case of four S/C observations having been available, three equations of the type Eq(1) were used to determine $\hat{n}_d$ and V_d. This case was completely kinematically determined from the geometric configuration and onset times alone.

For a few cases that were well known to be shocks, and when plasma data were available, one of the best-fit methods using a subset of the shock conservation equations was employed to obtain $\hat{n}_s$ (Chao, 1970; Lepping and Argentiero, 1971).

The normal $\hat{n}_d$, computed from the multiple S/C method, was compared with both $\hat{n}_t$ and $\hat{n}_s$, obtained from the single S/C magnetic field measurements. And when available the solar wind speed was compared to the estimated discontinuity speed divided by the radial component of the unit normal. It is, in general, possible to differentiate a shock wave

from a tangential discontinuity by these comparisons. Well known shock and tangential discontinuity signatures in the magnetic field data (Burlaga, 1968) also may be used as a guide in the discrimination. By combining the single and multiple S/C methods, it was possible in general to lessen the uncertainty of the estimate of the normal of the discontinuity, yielding final errors usually of approximately $\pm$ 10°. The preceeding scheme and assumptions form the basis for the method used to obtain the identification and kinematic properties of the discontinuity.

The Observations

For the active period of the solar cycle from 1968 to 1971 inclusive, we selected 93 world-wide SSC's which have been reported by more than 20 geomagnetic stations each (Solar-Geophysical data, published by ESSA, U.S. Department of Commerce). Then the solar activity which occurred one to four days before the SSC's were examined. The SSC's usually could be associated with a flare of importance 1B or stronger and radio bursts of Type II and Type IV. On an average the solar activity association of these events can be made with a reasonable degree of certainty, as we will demonstrate in a later section.

Of the 93 SSC's 81 could be associated with solar activity. Eighty-five percent of these associations included radio bursts of Type II or Type IV. Therefore, we believe our statistics of these 81 events are significant.

The IP magnetic field data from the S/C listed in Table 1 were available for 48 of the 93 SSC events. From these IP data our analysis shows 7 of the 48 events were tangential discontinuities and the remaining

41 were shock waves. However, only 38 of these 41 shocks had adequate IP data to obtain shock normals and speeds.

Chao (1973) has shown two examples of IP shock-like discontinuities which had a "shock" transition region of a thousand proton Larmor radii or wider. These two events steepened into shock waves in the vicinity of the earth. These two "shocks" can be associated with solar flares and with radio bursts of Type II and Type IV. We examined the thickness of the magnetic field transitions of the 38 shocks and found that 30% of the "shocks" had a transition region larger than 50 proton Larmor radii, R_p. In most of the thick-structure events, the transition regions were more than a few hundred R_p in width. We do not claim that the events with a thick transition zone are fully formed shocks. We would like to suggest that what we are observing in these cases is the formation of shocks.

Out of the 38 shocks, 22 shock normals and speeds were computed accurately, and their solar activity associations were relatively reliable. We will study IP shock correlation with solar activity using these 22 events. Table 2 gives a summary of the results discussed in this section.

Results

If we assume that the 81 flare-associated events represent disturbances such as shock waves propagating over 1 AU from the flare site to the earth's vicinity, then the average transit velocity of such a disturbance can be computed using the difference between the occurrence of the flare and the onset of the SSC at earth. A histogram of these mean speeds is given in Figure 1. There is a peak at 600 - 700 km/sec. The

Table 2

Some Statistics of SSC-Associated Events

Period of Study: January 1968 to December 1971

93 world-wide SSC's were selected.

81 of the SSC's were associated with flares and in some cases radio bursts (Type II and/or IV).

48 had available interplanetary (IP) magnetic field and in some cases plasma data for the associated IP events.

Analysis of 48 IP events yielded:

7 tangential discontinuities

41 shocks
- 3 had unknown normals and speeds.
- 38 had known normals and speeds:
  - 26 were thin structures
  - 12 were thick structures

22 of the 38 shocks had accurate shock normals and speeds estimated and all 22 were flare associated.

distribution in the upper and lower speed portions may not be reliable due to the difficulty of selection for the extremes. However, the peak of the distribution is significant. This mean speed of 600-700 km/sec implies that the shock speed is not on an average very much greater than the solar wind speed, i.e., the shock is of intermediate strength.

The shock normals of the 38 shocks are shown in Figure 2. The normals are given in solar ecliptic coordinates where Θ_{SE} is the latitude angle and ϕ_{SE} is the azimuth angle measured in the ecliptic plane. The dotted arrows represent those events with larger uncertainties than those with solid arrows; the latter set (22 shocks) usually correspond to multiple spacecraft observations and are well determined. These normals are rather symmetrically distributed with respect to the sun-earth line.

For those 15 of the 38 shocks for which plasma data were available the dependence of the shock speed in the solar wind frame of reference on the local solar wind speed in the pre-shock state was studied. Figure 3 shows the local shock speed in the solar wind frame, W, versus the solar wind speed V_{SW}. The figure shows that the pre-shock solar wind speeds occur in the range 350 to 420 km/sec, which corresponds to the most probable solar wind conditions. W, however, ranges from 40 to 300 km/sec.

Next, we compare the mean shock speed with the local shock speed as computed by the multiple spacecraft method. Figure 4 shows a plot of the mean transit velocity $\langle V_S \rangle$ versus the local shock speed V_S. Notice that most of the events lie below the diagonal line. That is, the mean speed $\langle V_S \rangle$ is larger than V_S for most events. This shows that, in general, flare-produced shocks slow down during propagation over 1 AU.

The orientation of shock normals and their positions relative to the parent flares can be studied to obtain an average shock front. Individual locally-determined shock surface orientations may severely deviate from this front (Lepping and Chao, 1972). The 22 shock events (for which normals have been accurately computed), their normals, and information about the identification of the probable parent flares are listed in the top section of Table 3. The remaining 16 of the 38 shocks are listed at the bottom of the table. The first two columns give the dates and times of the SSC events, respectively. The third column gives the Code number which identifies each event. The fourth through eighth columns give the following for each flare: the time of onset, position in latitude, importance, and the time of onset of radio bursts of Type II and Type IV, respectively. The next three columns give the shock normal in solar ecliptic coordinates θ_s and ϕ_s ($\phi_s = 0°$ in the solar direction), and the local speed computed from the multiple S/C method, respectively. The average sun-earth transit speed is given in the last column.

These 22 events are related to their parent flares in Figure 5 according to a method by Taylor (1969), and recently repeated by Bavassano et al. (1973) using the Pioneer 8 data. Figure 5 is a plot of the orientations of the 22 shock surfaces in the ecliptic plane at the appropriate heliocentric longitude relative to the flare. The longitudes are specified as seen from the earth. For example, the flare associated with the SSC of November 20, 1968 occurred at 90°W on the solar disk and thus is plotted at 90°E of the flare as shown in the figure (Code no. 19). This figure shows that the average shock surface in the ecliptic plane

Table 3

List of 38-Flare-Associated Shock Waves

Ground Data		Code Number	Probable Flare			Importance	Radio Bursts		Shock Normal		Speed	Mean Speed
Date	U.T.		Date	U.T.	Position		Type II UT	Type IV UT	Θ_s (degree)	Φ_s (degree)	(km/sec)	(km/sec)
1-11-68	1250	1	1-9	0507	N09E28	2B	----	----	-5.3	152	490	740
1-26-68	1440	2	1-22	0440	S20W23	1B	----	----	-20	153	513	390
2-10-68	1620	3	2-8	1402	S13W14	1B	1402	----	41	166	500	830
2-14-68	1253	4	2-10	1622	S17E55	2B	1631	1632	14	210	480	440
2-20-68	0704	5	2-17	0248	N17W47	1B	0259	----	-51	163	300	540
5-07-68	0030	7	5-3	2123	N19E50	1B	2127	2131	-1	210	400	550
7-13-68	1612	10	7-8	1707	N13E59	3B	1708	1710	-15	154	500	440
8-23-68	1713	11	8-21	0146	S16W44	1B	0154	----	31	190	480	650
9-30-68	2345	13	8-29	1616	N16W52	3B	1619	1619	33	208	280	1330
10-6-68	0628	14	10-3	2348	S16W37	3B	2359	----	26	195	650	750
10-29-68	0908	16	10-26	0130	S20E32	1N	0132	----	-22	189	420	520
11-16-68	0915	18	11-12	1421	N05W73	2B	----	----	5	178	480	450
11-20-68	0904	19	11-18	1026	N20W90	2N	1026	1026	-42	153	370	880
2-26-69	0155	25	2-24	2305	N12W31	2B	2311	2310	-14	159	360	1570
3-17-69	0030	26	3-13	2117	S14E50	-B	2117	----	-7	153	550	550
6-17-70	0750	57	6-14	1324	N22E42	3B	1328	1329	-18	167	480	620
7-3-70	2250	62	7-1	2022	N18W16	1B	2044	2044	26	130	500	830
7-8-70	2317	63	7-6	2137	N22W90	1B	2140	----	11	176	500	830
7-29-70	0043	66	7-26	0637	N08W28	2B	----	----	-4	188	510	630
4-9-71	0428	78	4-6	0936	S19W80	1B	----	----	25	195	400	620
4-21-71	1628	80	4-19	1223	S21W06	2B	----	----	0	178	475	790
5-17-71	0628	82	5-14	1411	N03E15	3B	1415	1411	0	174	510	650
11-1-68	0915	17	10-29	0859	S13W09	2B	----	----	37	176	500	560
2-10-69	2021	24	2-8	1200	N12E02	1B	1207	1205	-4	204	410	450
3-19-69	1958	27	3-16	2334	N13E19	-1	2340	----	0	259	450	550
3-23-69	1825	28	3-21	1312	N18E10	2B	1319	1319	6	166	495	780
7-26-69	1152	35	----	----	------	--	----	----	-39	119	430	---
9-5-69	1333	37	9-4	0825	N05W53	1B	----	----	-18	183	---	1400
9-14-69	1518	38	9-13	0111	S32W47	2N	----	----	-53	192	---	1000
9-27-69	2124	39	9-25	1425	N05W39	1B	----	1427	54	165	---	670
10-18-69	2029	42	----	----	------	--	----	----	27	189	---	---
6-1-70	0305	55	5-30	0424	S10W35	3F	----	----	-51	134	---	880
6-27-70	0605	59	6-25	0759	S08W25	3B	----	----	-41	157	400	570
8-16-70	2204	67	8-14	1556	N16W74	2B	----	1600	26	132	---	750
3-19-71	1149	76	----	----	------	--	----	----	-52	147	440	---
4-3-71	2139	77	4-1	1319	S17W14	3N	----	1325	-15	230	460	740
4-14-71	1242	79	4-11	----	------	--	----	1433	76	185	---	600
5-30-71	0736	83	5-26	----	-------	--	----	1535	0	191	470	470

near the earth's orbit lies on a circle centered at the sun with a radius of 1 AU. A few events have been observed near the west limb but these also lie well on the circle. The mean deviation of these shock surfaces from the circle is 5° (± 9°), i.e. $\langle \phi_s \rangle$ = 175° for the average normal, with a standard deviation (σ) from the mean surface of about 22°. The mean deviation of the remaining 16 shock surfaces from the circle is 3° (± 18°) and $\sigma \approx 36°$. This is somewhat different from the results given by Hirshberg (1968), Taylor (1969) and Bavassano et al. (1973) which suggest smallar radii of curvature by approximately a factor of 2.

Figure 6 shows the orientation of the 22 shock surfaces in the meridional plane at the appropriate heliocentric latitude relative to the flare position. The shock surfaces are clumped above and below the ecliptic plane at about ± 20°. The figure shows that there is a tendency for the average shock surface in the meridional plane near the earth's orbit also to lie on a circle centered at the sun with a radius of 1 AU. The mean deviation of these shock surfaces from the circle is 0.6° (± 10°) with a σ of about 24°. For the remaining 16 shocks the corresponding values are 3° (± 20°) and 39°, respectively. This implies that the average shock surface does not deviate much from a spherical shape in the meridional plane.

Using the 22 flare-associated shock waves, we obtained statistics about the correlation between shock waves, flares and radio bursts of Type II and Type IV. Table 4 gives the probability of solar activity being associated with interplanetary shock waves. We have divided the solar activity into three classes, namely: flares, radio bursts of

Table 4

Flare and Radio Bursts-Associated Interplanetary Shock Waves

Type of Associations	Percentage of Interplanetary Shocks
Flare, Type II and IV	45%
Flare, Type II	75%
Flare, Type IV	55%
Flare only	15%
Flare, Type II or IV	85%

Table 5

Flare and Radio Bursts-Associated Interplanetary "Random" Shock Waves

Type of Associations	Percentage of IP Random Shocks
Flare, Type II and IV	20%
Flare, Type II	40%
Flare, Type IV	30%
Flare only	50%
Flare, Type II or IV	50%

Type II and Type IV, which are believed to be most strongly related to interplanetary shock waves (Wild, 1970). From this table one can see that, of radio bursts, Type II have the stronger correlation with IP shocks. Note that in general one can always find a flare-association with a given IP shock, because there are so many flares reported over any four day period. On the other hand, if the radio data are included, it is seldom possible to make more than one association with a given IP shock. This table shows that we apparently do have a meaningful association with IP shocks and solar activity.

In order to test our method of associating solar flares with the observed IP shocks, we artificially generated random IP shock times and repeated the association procedure as if the times were real shock onsets (or SSC's) at 1 AU. The day of occurrence was generated by computer assuming a uniform distribution and an expected rate of 2 shocks per month for 2 years (1968-1969). The hour of day was derived by throwing a die so that resulting "onset times" had a quantization of 4 hours duration. (Over a large number of throws the value showing on the die is expected on average to be 3-1/2; in our case of 48 throws it was 3.46.) Using these times we attempted to associate solar flares, Type II-, and/or Type IV-solar bursts just as we had done in the cases of the real IP shocks. For all but two random shocks we were able to find some flare association. For these 46 cases a histogram of mean speeds was produced as shown as a solid curve in Figure 7, corresponding to Figure 1 for the real cases. In some instances radio bursts were associated, and the percentage of these associations is shown in Table 5, corresponding to

Table 4 for the real cases. For some of the associations it was necessary to ignore the more impressive solar flare, by importance designation, in favor of a lesser flare because of the existence of radio bursts, Type II and/or IV at the time of the lesser flare. This was also done in the real cases but not as frequently. Firstly, we point out that the histogram in Figure 7 (solid line) shows a skewed distribution with respect to the histogram in Figure 1, which is shown in Figure 7 as a dashed curve, properly scaled, for comparison. Secondly, the most probable speed is shifted to an unrealistically low value of $\approx$ 500 km/sec, instead of 650 km/sec for the real cases. (The average post shock solar wind speed alone over 1 AU is expected to be greater than 500 km/sec). Thirdly, and most important, as Tables 4 and 5 show, the percentage of occurrences of solar radio bursts in any combination is much lower than in the real cases. In particular compare Flare, Type II or Type IV for random (50%) to real cases (85%). Also the flare importance designation was necessarily lower, on an average, for the random case associations. Lastly, we point out the difference of the mean speed averages but the similarity of the σ's, as Table 6 shows. We conclude that the method of using an IP shock-solar association based on Flares, and Type II and IV bursts when present, for this statistical study yielded reasonably trustworthy results. But we caution that one must be exceedingly careful about <u>individual</u> shock studies based on such a method.

<u>Some Flare-Shock Properties</u>

In this section we list and discuss those properties of oblique IP flare-shocks which depend explicitly on magnetic field quantities and

Table 6

Characteristics of Mean Speed Distributions

	No. of Events (N)	Ave $\pm$ Error $\left(\frac{2\sigma}{\sqrt{N}}\right)$	σ
		in km/sec	
Random Test	46	660 $\pm$ 70	240
Real Cases	82	790 $\pm$ 50	230
Difference		130 $\pm$ 90	10

shock normals only, based on the shocks in Table 3, top. In particular we are concerned with giving a general characterization of typical magnetic field jumps across such shocks. And we are interested in the expected importance of thermal anisotropy on estimating shock parameters and normals using a fitting scheme based on shock conservation equations (Lepping and Argentiero, 1971). Also we wish to check the accuracy of the estimated normals presented in this paper. Only the most accurate set, according to the shock normal estimates, of the 22 shocks will be examined. These shocks will be characterized by the quantities defined in Table 7. In the table column-number referes to the respective column in Table 8, where the results are presented. The parameter R in column 7 provides a means of measuring the importance of anisotropy (Lepping, 1972). That is, for $0 \leq R \leq 1/2$ and for expected anisotropy conditions in the vicinity of the interplanetary shock (Hundhausen et al., 1967; Chao and Goldstein, 1971) departure from the assumption of thermal isotropy is in genral unnecessary (Lepping, 1972). Below we show that indeed $R \leq 1/2$. Concerning column 9, $\Delta\vec{B} \cdot \hat{n} = 0$ must be satisfied across the shock; checking it gives the degree of consistency of estimated normals with this constraint, where $\delta = 0°$ indicates perfect agreement. S and S_o are arbitrarily defined measures of the "probable strength" of the shock when plasma data is unavailable; F_2/F_1, is a similar indicator. All other quantities in the Table 7 are self-explanatory.

These quantities were calculated for the 22 shocks and the results are presented in Table 8. In obtaining these results the following rules were applied. Only data from one S/C were used, $\alpha \geq 10°$, $\delta \leq 10°$,

Table 7

Definitions of Characteristic Quantities

of 22 Flare-Shocks

Column	Quantity
1	Code number refers to an event in Table 3.
2	S/C = spacecraft's data that was used.
3	$\theta_1 = \measuredangle(\hat{n}, \vec{B}_1)$
4	$\theta_2 = \measuredangle(\hat{n}, \vec{B}_2)$
	where $\hat{n}$ is the shock normal and 1 and 2 are pre- and post-shock, respectively.
5	$\alpha = \measuredangle(\vec{B}_1, \vec{B}_2)$
6	$\theta_1 + \alpha$
7	$R = \tan\theta_1/\tan\theta_2$
8	F_2/F_1 where $F_i = \sqrt{B_{ix}^2 + B_{iy}^2 + B_{iz}^2}$ $\quad i = 1,2$
9	$\Delta\vec{B} = \vec{B}_2 - \vec{B}_1$; $\delta = 90° - \cos^{-1}(\hat{n} \cdot \frac{\Delta\vec{B}}{\lvert\Delta\vec{B}\rvert})$.
10	$S = 2\left(\frac{F_2 - F_1}{F_2 + F_1}\right)$, for F_i see 8 above.
11	$S_o = \frac{F_2 - F_1}{F_1}$, for F_i see 8 above.

Table 8

Characteristics of 18 Flare-Shocks

Code	S/C	β_1	β_2	α	$\beta_1 + \alpha$	R	F_2/F_1	δ	S	S_o
1	33	61°	85°	25°	86°	0.18	3.3	4.0°	1.07	2.29
2	35	60°	76°	16°	76°	0.43	2.2	1.3°	0.75	1.20
3	33	43°	80°	37°	80°	0.16	2.5	8.1°	0.86	1.50
4	33	57°	67°	10°	67°	0.68	1.4	0.2°	0.30	0.35
10	34	22°	49°	39°	61°	0.35	1.4	0.8°	0.32	0.38
11	34	33°	57°	24°	57°	0.43	1.5	1.7°	0.40	0.50
13	34	48°	65°	26°	74°	0.52	1.9	7.4°	0.64	0.94
14	34	41°	74°	33°	74°	0.25	2.8	0.8°	0.94	1.76
16	35	38°	72°	33°	71°	0.26	2.5	1.2°	0.87	1.53
18	34	55°	77°	22°	77°	0.34	2.1	4.9°	0.69	1.06
19	34	66°	85°	19°	85°	0.19	3.6	1.6°	1.13	2.58
25	35	36°	62°	26°	62°	0.39	1.7	1.3°	0.54	0.74
26	35	40°	62°	22°	62°	0.45	1.6	0.8°	0.48	0.63
57	41	45°	67°	22°	67°	0.42	1.8	0.8°	0.58	0.82
62	41	70°	82°	12°	82°	0.38	2.5	0.1°	0.87	1.53
63	41	44°	72°	27°	71°	0.32	2.3	0.7°	0.78	1.29
66	41	52°	67°	15°	67°	0.54	1.6	0.6°	0.45	0.59
78	41	38°	62°	25°	63°	0.41	1.7	3.9°	0.50	0.67

and where a close choice had to be made among different S/C the event with the smallest δ and/or largest α was chosen, where judicious weighting between these rules was used on occasion. Only 18 shocks remain out of 22, as the table shows. Only two of the discarded cases (Codes 5 and 7) were due to the possibility of inaccurate normals (δ = 23° and 68°, respectively) but most likely were due to poorly determined $\Delta\vec{B}$'s. (Code 7 refers to a thick "shock" and undoubtedly had a rather poorly determined $\Delta\vec{B}$ but probably a good normal.) The other 2 cases (Codes 80 and 82) arose because of small α. This was due to the shocks being nearly perpendicular types ($\theta_1 \approx 85°$), and our interest in this section is in oblique shocks. Ideally $\theta_2 = \theta_1 + \alpha$ according to the magnetic coplanarity theorem. Comparing columns 4 and 6 shows that this closely holds in almost every case; one should note that this result was not forced (by a circular argument), since the associated normals for these shocks were almost exclusively obtained by multiple S/C methods.

The table shows that in almost all cases $R \lesssim 1/2$ and for this set a typical value is $R \cong 1/3$, the average being 0.37. The particular values of θ_1 shown occur partly by selection, but it is interesting that α rarely exceeds 35°— and recall that S/C data giving small α were discarded for this table. It is not obvious which of the three parameters F_2/F_1, S, or S_o best reflects probable shock strength, without accompanying plasma data, but the obvious inverse relationship between R and F_2/F_1 is intriguing. Figure 8 shows a plot of F_2/F_1 vs. R for these 18 shocks.

The figure suggests the statistical relationship (with a least squares rms = 0.39):

$$F_2/F_1 \cong 3.5 - 3.7\ R \qquad (3)$$

where $R \equiv \tan \theta_1/\tan \theta_2$. Chao (1970) demonstrates that

$$\frac{F_2 \sin \theta_2}{F_1 \sin \theta_1} = \frac{M_A^2 - 1}{M_A^2(N_1/N_2)-1}\ , \qquad (4)$$

for a thermally isotropic medium, where M_A is the pre-shock Alívén Mach number and N is the plasma number density. Since the normal component of the magnetic field across the shock front is continuous, i.e. since $F_2 \cos \theta_2 = F_1 \cos \theta_1$, Eqs. 3 and 4 can be combined to yield

$$M_A \cong \sqrt{\frac{F_2/F_1 + 0.2}{3.7\ N_1/N_2 + F_2/F_1 - 3.5}} \qquad (5)$$

Hence, the strength of an oblique IP shock at 1 AU for the isotropic assumption depends, in a statistical way, only on the scalar quantities F_2/F_1 and N_1/N_2. In general the empirical relationship given by Eq.(5) may not be very accurate for any particular shock, but it suggests a typical property of oblique IP shocks at 1 AU. However, we tested it for several previously studied specific shocks which were parameter-fitted according to schemes developed by Chao (1970) and Lepping and Argentiero (1971), and it yielded estimates of M_A which when compared to best-fit values gave discrepancies ranging from 30% to only 10%. It appears that when N_1/N_2 gets too small (say $\lesssim 0.3$) relationship (5) yields unreliable estimates of M_A.

Discussion

Firstly, we would like to point out that our criterion for selecting SSC's, which was based on the agreement of reports from 20 or more magnetic

observatories, was consistent with assuming SSC events are caused by interplanetary shocks. From 48 events for which interplanetary magnetic field and/or plasma data were available, only 15% were caused by tangential discontinuities. For a continuation of the study described above and for completeness we relaxed our criterion for SSC-selection by including also those events identified by only a few (5 to 10) observatories. In those cases less than approximately 15% of the SSC's were caused by IP shocks; the identification of these IP events was not always unambiguous. The results of the extended study are not reported here. Hence, large and universally observed SSC's tend overwhelmingly to be caused by IP shocks, and the lesser "SSC's" also may be caused by IP shocks but more likely by tangential discontinuities and other solar wind inhomogeneities.

Secondly, we wish to stress the distinction between this statistical study and detailed studies on a single shock surface geometry (Mariani et al. 1970; Lepping and Chao, 1972). Figure 5 suggests that the average shock surface near the earth's orbit lies on a circle centered at the sun with a radius of 1 AU. However, the standard deviation from the mean surface is about 22°. This indicates that an individual shock surface geometry can deviate rather markedly from a spherical shape. From a physical point of view a spherically symmetric shock near the sun propagating through IP space will interact with interplanetary discontinuities (Lepping and Burlaga, 1973) and IP large scale inhomogeneities, such as streams and gradients in density, temperature, velocity, etc. (Heinemann and Siscoe, 1973). That is, it appears that an individual shock front may be distorted not only in gross geometry from a spherical shape,

but also experience a "rippling" on the scale of the correlation length of IP tangential discontinuities. A collection of these various perturbations on shock surfaces may result in an ensemble average of such surfaces being spherical with a relative large standard deviation even though few of the individual shock surfaces were actually spherical. In this sense the RMS deviation of the normals is probably more important than their average.

Figures 5 and 6 (especially 5), showing a tendency for a radius of curvature of 1 AU at 1 AU regardless of the location of the flare site with respect to the shock observation point, tend to suggest that the initial (solar) shock shape is less important than IP processes in causing shock normal scattering over 1 AU ($\sigma \approx 23°$). In fact, the symmetry indicated by these figures is rather remarkable from the viewpoint of IP shock normals. However, an equally striking <u>asymmetry</u> exists which suggests a relationship about IP shock survivability. Notice that of the 33 shocks listed in Table 3 having a flare site association, 11 have an East solar longitude designation but 22 have a West designation. That is, it appears that an observer at 1 AU is twice as likely to find shocks related to West longitude flares as East longitude; the average for the set of 33 flares is 17°W. Even the limited set of 22 shocks (Table 3, top, and Figure 5) give essentially the same results: 14 West longitude and 8 East longitude. Sakurai (1973 a,b) finds an apparently related asymmetrical tendency also based on SSC-flare associations: his statistical study shows that a maximum mean speed direction lies ≈ 30°W of the central meridian of the solar disk, i.e. near to the mean spiral

direction. The IP shock geometry for the Feb. 15-16, 1967 shock discussed by Lepping and Chao (1972) indicates a strong similarity. It appears that a shock experiences a greater chance of survival beyond 1 AU if it propagates along a direction approximately parallel to that average spiral which maps back to the flare site. This is not unreasonable according to the model by Heinemann and Siscoe (1973), which crucially depends on the IP spiral geometry and on large scale interactions of IP shocks with streams. The meridional plane statistics are less interesting: 19 North latitude and 14 South latitude for the set of 33 shocks, and 13 North and 9 South for the set of 22 shocks.

In conclusion, interplanetary shock waves and geomagnetic storm sudden commencements (SSC's) are correlated with the solar activity of flares, radio bursts of Type II and/or Type IV. The average IP shock front at 1 AU has a radius of curvature on the order of 1 AU. However, the geometry of the shock front deduced to be of spherical shape is obviously not representative of any individual event, because an individual shock front may be severely distorted over 1 AU by IP processes.

Acknowledgements

We are indebted to Dr. L. F. Burlaga for suggesting that we undertake this work and we thank him and Dr. K. W. Ogilvie for helpful comments and criticisms.

We would like to thank the investigators listed in Table I and their associated groups for the use of their magnetic field and solar plasma data.

Also we are grateful to Dr. K. Sakurai for his help in making some of the radio burst associations with the SSC events, and to Dr. G. L. Siscoe for suggesting the simulated random-shock study.

References

Bavassano, B., F. Mariani, and N. F. Ness, Pioneer 8 Observations and Interpretations of 16 Interplanetary Shock Waves Observed in 1968, J. Geophys Res., 78, 4535, 1973.

Burlaga, L. F., Micro-Scale Structures in the Interplanetary Medium, Solar Phys., 4, 67, 1968.

Burlaga, L. F. and N. F. Ness, Tangential Discontinuities in the Solar Wind, Solar Phys., 9, 467, 1969.

Chao, J. K., Interplanetary Collisionless Shock Waves, M.I.T. Report CSR TR-70-3, February 1970.

Chao, J. K., Steepening of Nonlinear Waves in the Solar Winds, J. Geophys. Res., 78, 5411, 1973.

Chao, J. K. and B. E. Goldstein, Thermal Anisotropies in the Vicinity of Solar Wind Shocks, M.I.T. Report CSR-P-71-53, February 1971.

Colburn, D. C. and C. P. Sonett, Discontinuities in the Solar Wind, Space Science Rev., 5, 439, 1966.

DeYoung, D. S., and A. J. Hundhausen, Two-Dimensional Simulation of Flare-Associated Disturbances in the Solar Wind, J. Geophys. Res., 76, 2245, 1971.

Dryer, M., Some Effects of Kinetic Electrical Conductivity on Solar Flare-Induced Interplanetary Shock Waves, Cosmic Electrodyn. 1, 348, 1970.

Gold, T., Gas Dynamics of Cosmic Clouds, ed. by H. C. Van de Hulst and J. M. Burgers, North Holland Publishing Co., Amsterdam, P. 103, 1955.

Heinemann, M. A. and G. L. Siscoe, Shapes of Strong Shock Fronts in an Inhomogeneous Solar Wind, submitted to the J. Geophys. Res., 1973.

Hirshberg, J., The Transport of Flare Plasma from the Sun to the Earth, Planet. Space Sci., 16, 309, 1968.

Hirshberg, J., A. Alksne, D. S. Colburn, S. J. Bame, and A. J. Hundhausen, Observation of a Solar Flare Induced Interplanetary Shock and Helium Enriched Driver Gas, J. Geophys. Res., 75, 1, 1970.

Hundhausen, A. J., Solar Wind Disturbances Associated with Solar Activity, Intercorrelated Satellite Observations Related to Solar Events, p. 111, ed. by V. Manno and D. E. Page, D. Reidel, Dordrecht, Holland, 1970.

Hundhausen, A. J., S. J. Bame, and M. D. Montgomery, The Large-Scale Characteristics of Flare-Associated Solar Wind Disturbances, J. Geophys. Res., 75, 4631, 1970.

Hundhausen, A. J., S. J. Bame, and N. F. Ness, Solar-Wind Thermal Anisotropies: Vela 3 and IMP 3, J. Geophys. Res., 72, 5265, 1967.

Hundhausen, A. J. and R. A. Gentry, Numerical Simulation of Flare-Generated Disturbances in the Solar Wind, J. Geophys. Res., 74, 2908, 1969 (a).

Hundhausen, A. J. and R. A. Gentry, The Effects of Solar Flare Duration on a Double Shock Pair at 1 AU, J. Geophys. Res., 74, 6229, 1969 (b).

Korobeinikov, V. P., On the Gas Flow Due to Solar Flares, Solar Physics, 7, 463, 1969.

Lepping, R. P., Influence of Thermal Anisotrophy on Best-Fit Estimates of Shock Normals, J. Geophys. Res., 77, 2957, 1972.

Lepping, R. P. and P. D. Argentiero, Single Spacecraft Method of Estimating Shock Normals, J. Geophys. Res., 76, 4349, 1971.

Lepping, R. P. and L. F. Burlaga, Shock Scattering by Tangential Discontinuities in the Solar Wind, EOS 54, April AGU Abstract # 557, 439, 1973.

Lepping, R. P. and J. K. Chao, A Shock Surface Geometry: the February 15-16 1967 Event, NASA/GSFC X-692-72-433, September, 1972. (Submitted to J. Geophys. Res.)

Mariani, F., B. Bavassano, and N. F. Ness, Interplanetary Magnetic Field Measured by Pioneer 8 During the 25 February 1969 Event, Intercorrelated Satellite Observations Related to Solar Events, p. 427, ed. by V. Manno and D. E. Page, D. Reidel, Dordrecht, 427, 1970.

Ogilvie, K. W. and L. F. Burlaga, Hydromagnetic Shocks in the Solar Wind, Solar Phys., 8, 422, 1969.

Parker, E. N., Sudden Expansion of the Corona Following a Large Solar Flare and the Attendant Magnetic Field and Cosmic Ray Effects, Astrophys. J., 133, 1014, 1961.

Sakurai, K., Propagation Pattern of Interplanetary Shock Waves Associated with Solar Flares, NASA/GSFC X-693-73-90, April, 1973a.

Sakurai, K., On the Interplanetary Shock Waves Associated with Solar Flares in the Active Region McMath No. 9740, NASA/GSFC X-693-73-97, April 1973b.

Simon, M. and W. I. Axford, Shock Waves in the Interplanetary Medium, Planet. Space Science, 14, 901, 1966.

Taylor, H. E., Sudden Commencement Associated Discontinuities in the Interplanetary Magnetic Field Observed by IMP 3, Solar Physics, 6, 320, 1969.

Wild, J. P., Some Investigations of the Solar Corona: the First Two Years of Observation with the Culgoora Radio Heliograph, Proc. ASA., 1, 365, 1970.

Figure Captions

Figure 1 Distribution of mean transit speeds over 1 AU computed using the difference in time between the occurrence of the flare and the onset of the SSC at earth for 81 events.

Figure 2 The orientations of 38 shock normals. The angle Θ_s is the solar ecliptic latitude and ϕ_s is the solar ecliptic longitude. The dotted arrows represent events with larger uncertainties than those with solid arrows (see text).

Figure 3 W, the local shock speed in the solar wind frame versus the solar wind speed. $\vec{n}$ is an accurately estimated unit shock normal.

Figure 4 A comparison of the local shock speed and the mean transit speed.

Figure 5 Orientations in the ecliptic plane of the local shock surfaces at the appropriate heliocentric longitudes relative to their corresponding flares. The numbers associated with each event are the Code numbers (see Table 3).

Figure 6 Orientations in the meridional plane of the local shock surfaces at the appropriate heliocentric latitudes relative to their corresponding flares.

Figure 7 The distribution of mean transit speeds over 1 AU for simulated (random) cases (solid line) and for real cases (dashed line). The distribution of the real cases is the same as that in Figure 1, but has been properly scaled so that the total number of events equals 46.

Figure 8 F_2/F_1 vs R (= $\tan \beta_1/\tan \beta_2$, see Table 7) for 18 choice examples of flare associated shocks.

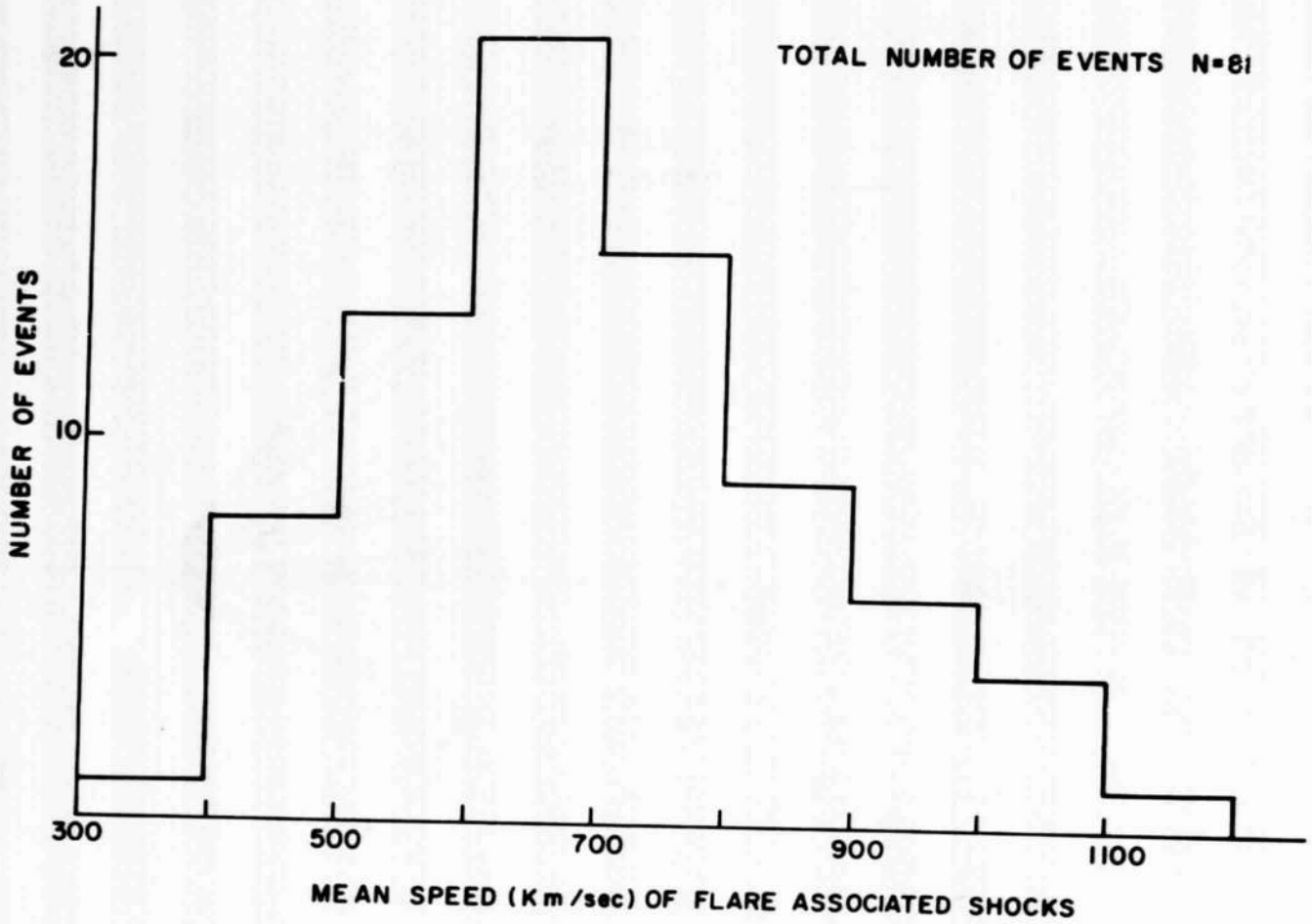
TOTAL NUMBER OF EVENTS N=81
NUMBER OF EVENTS
20
10
300
500
700
900
1100
MEAN SPEED (Km/sec) OF FLARE ASSOCIATED SHOCKS

Figure 1

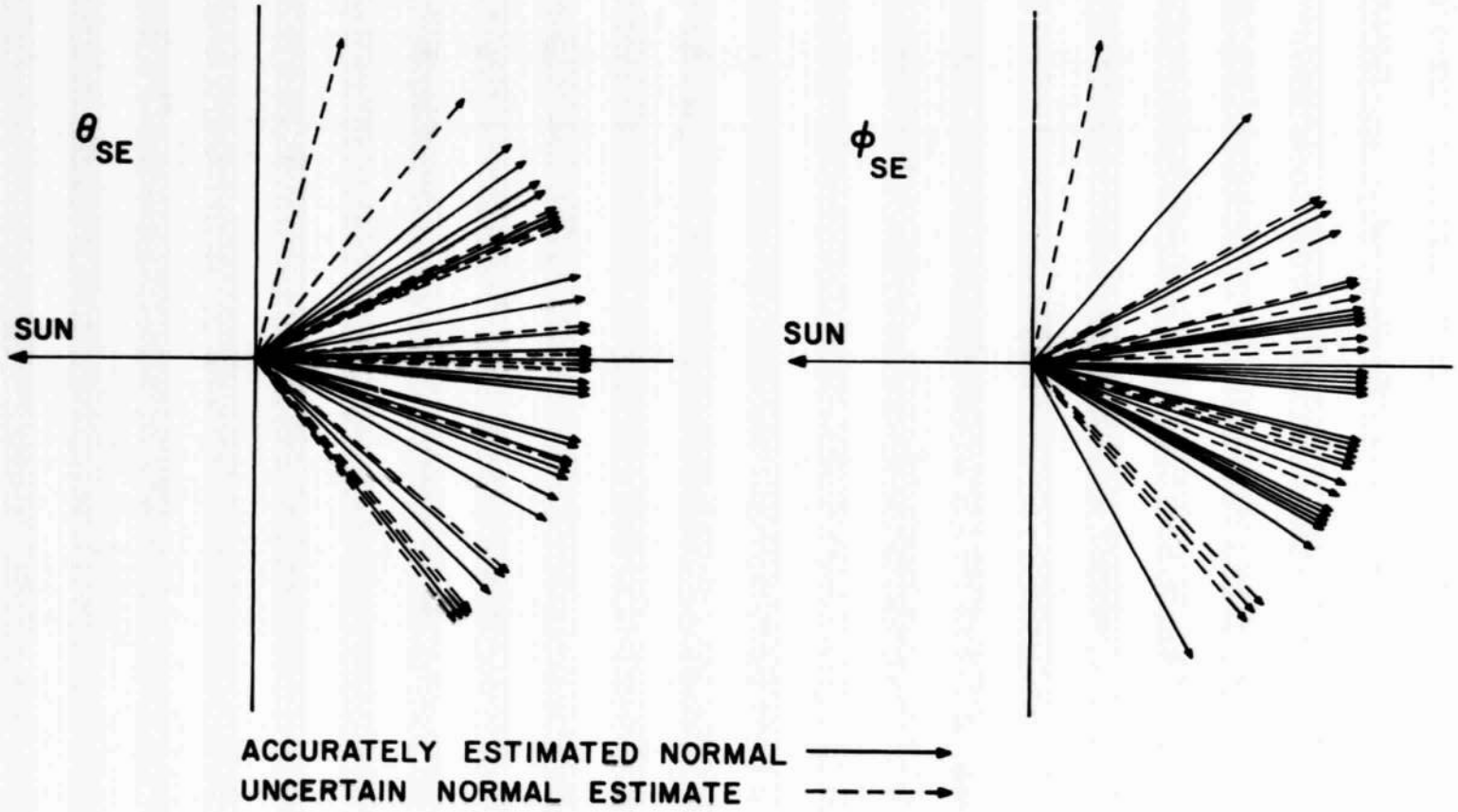
θ_{SE}
SUN
ϕ_{SE}
SUN
ACCURATELY ESTIMATED NORMAL
UNCERTAIN NORMAL ESTIMATE

Figure 2

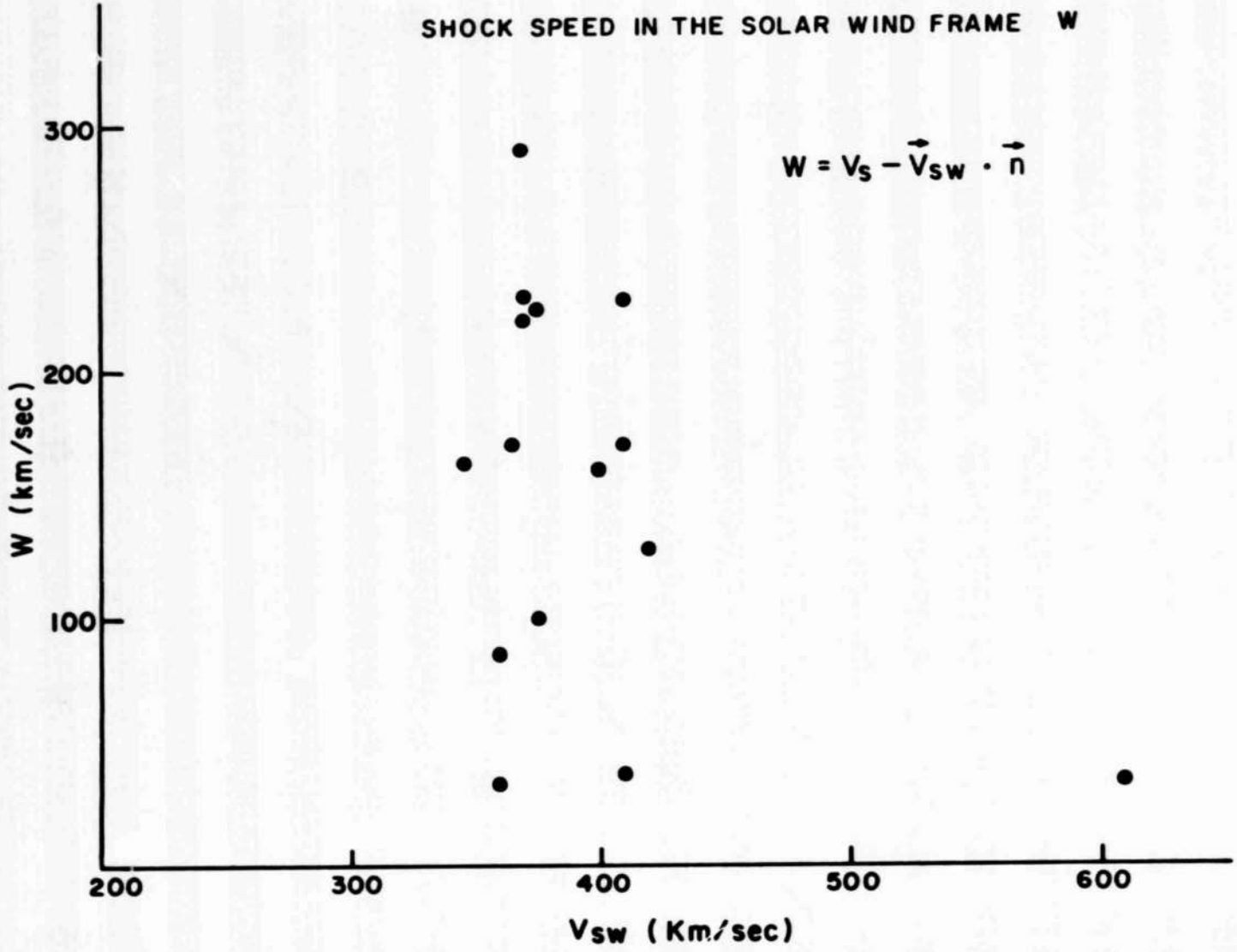
SHOCK SPEED IN THE SOLAR WIND FRAME W
$W = V_S - \vec{V}_{SW} \cdot \vec{n}$
300
200
100
W (km/sec)
200
300
400
500
600
Vsw (Km/sec)

Figure 3

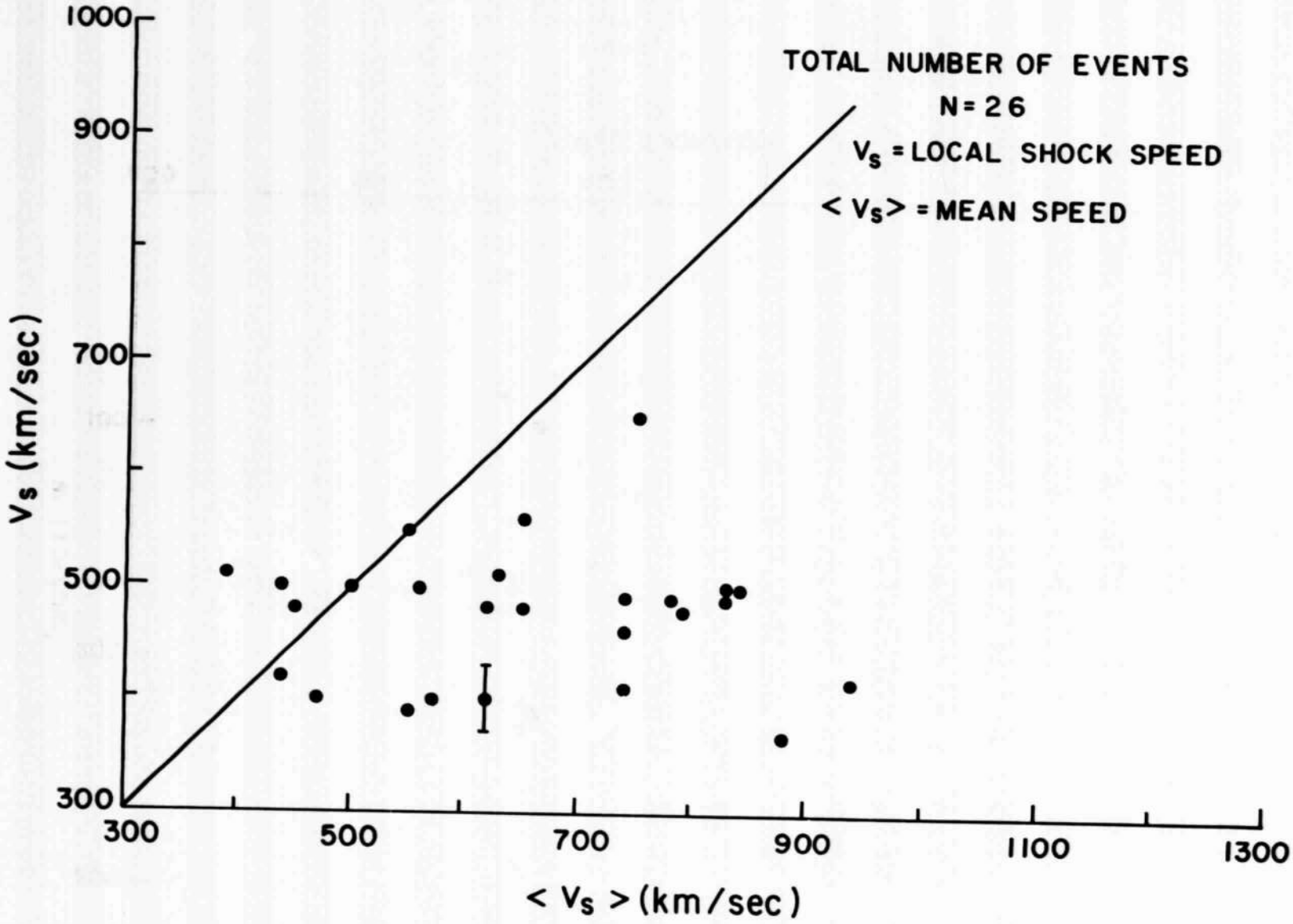
TOTAL NUMBER OF EVENTS
N = 26
V_s = LOCAL SHOCK SPEED
$< V_s >$ = MEAN SPEED
1000
900
700
500
300
V_s (km/sec)
300
500
700
900
1100
1300
$< V_s >$ (km/sec)

Figure 4

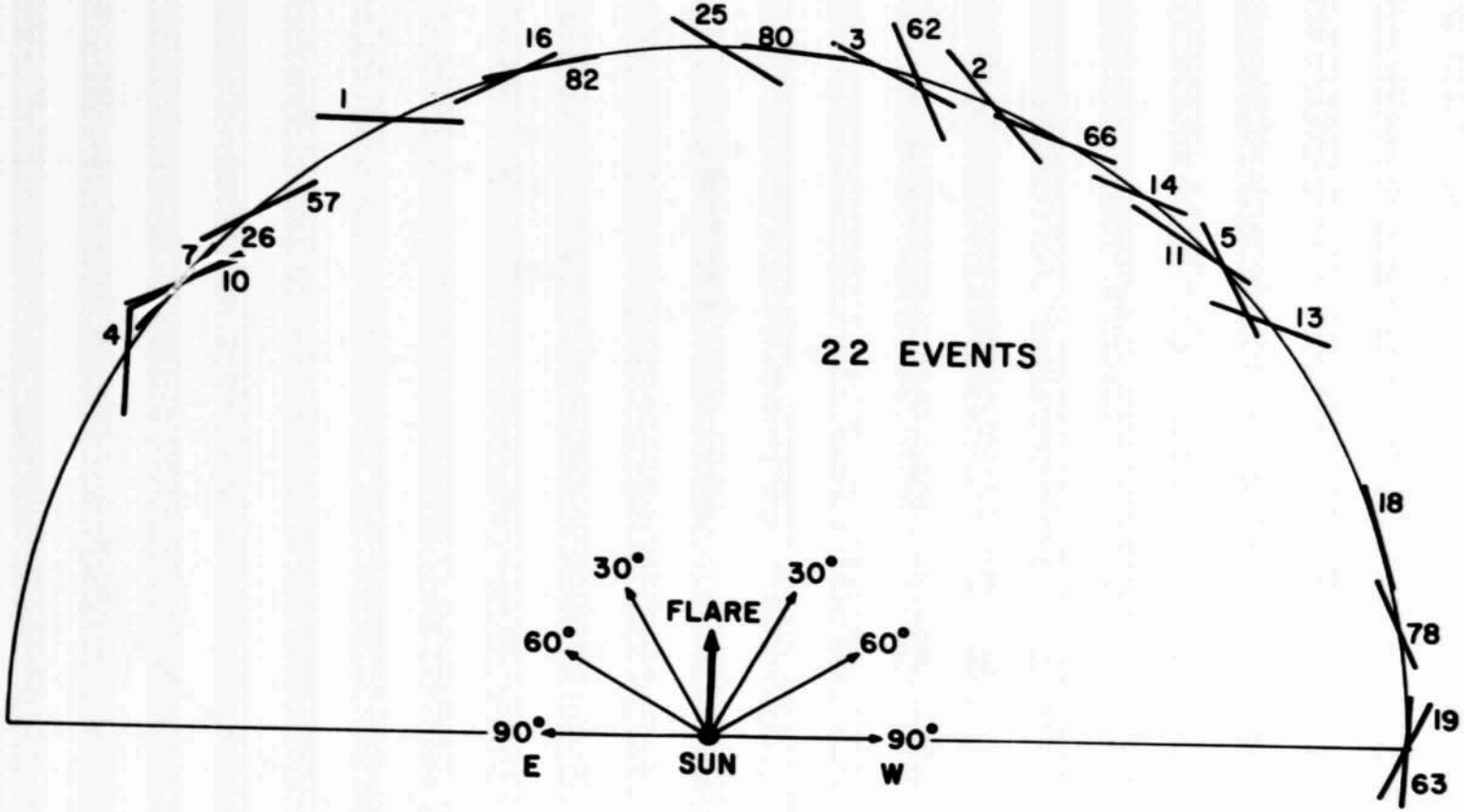
22 EVENTS
FLARE
30°
30°
60°
60°
90°
90°
E
SUN
W
1
16
82
25
80
3
62
2
66
14
5
11
13
18
78
19
63
4
7
26
10
57

Figure 5

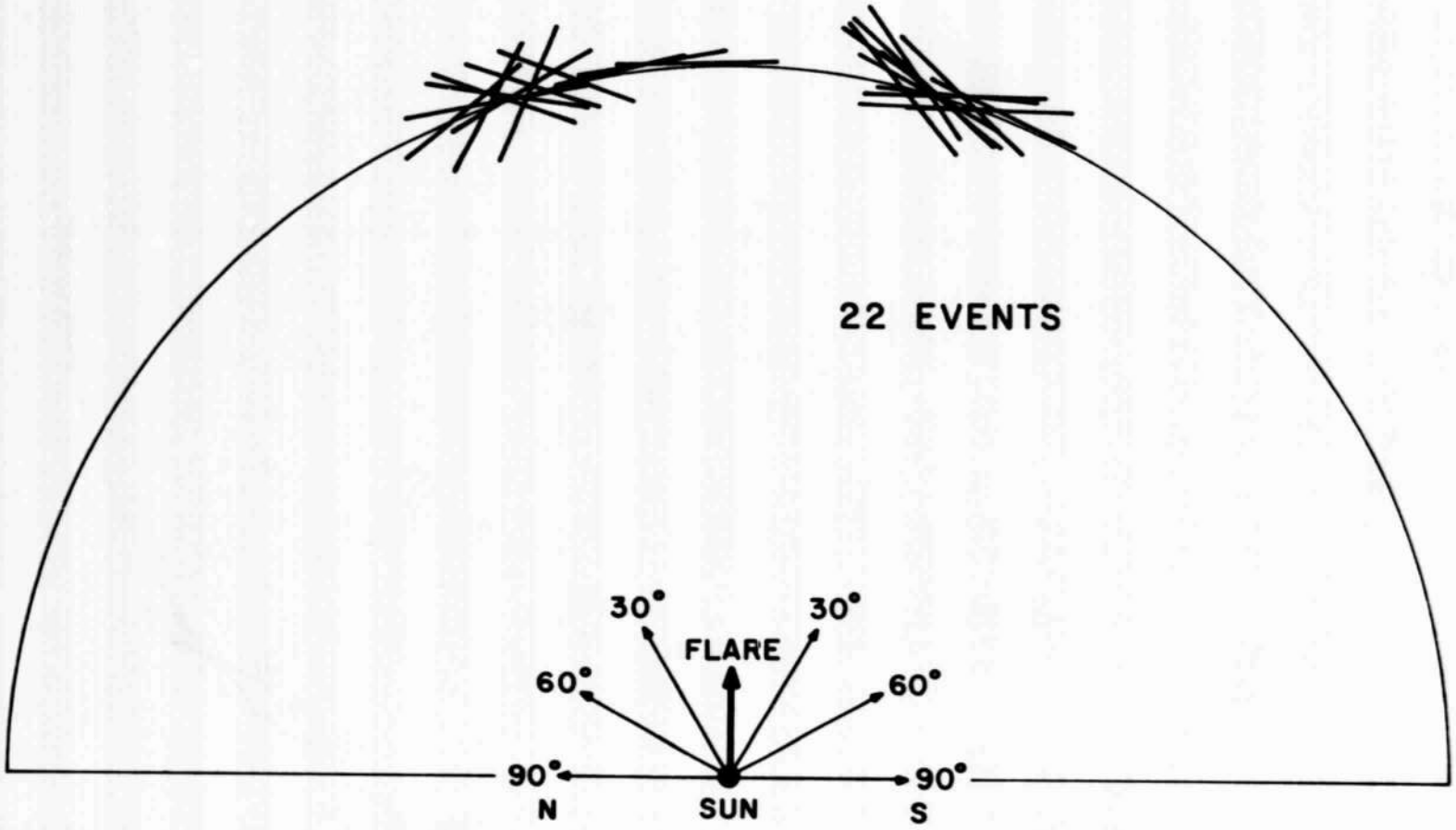

Figure 6

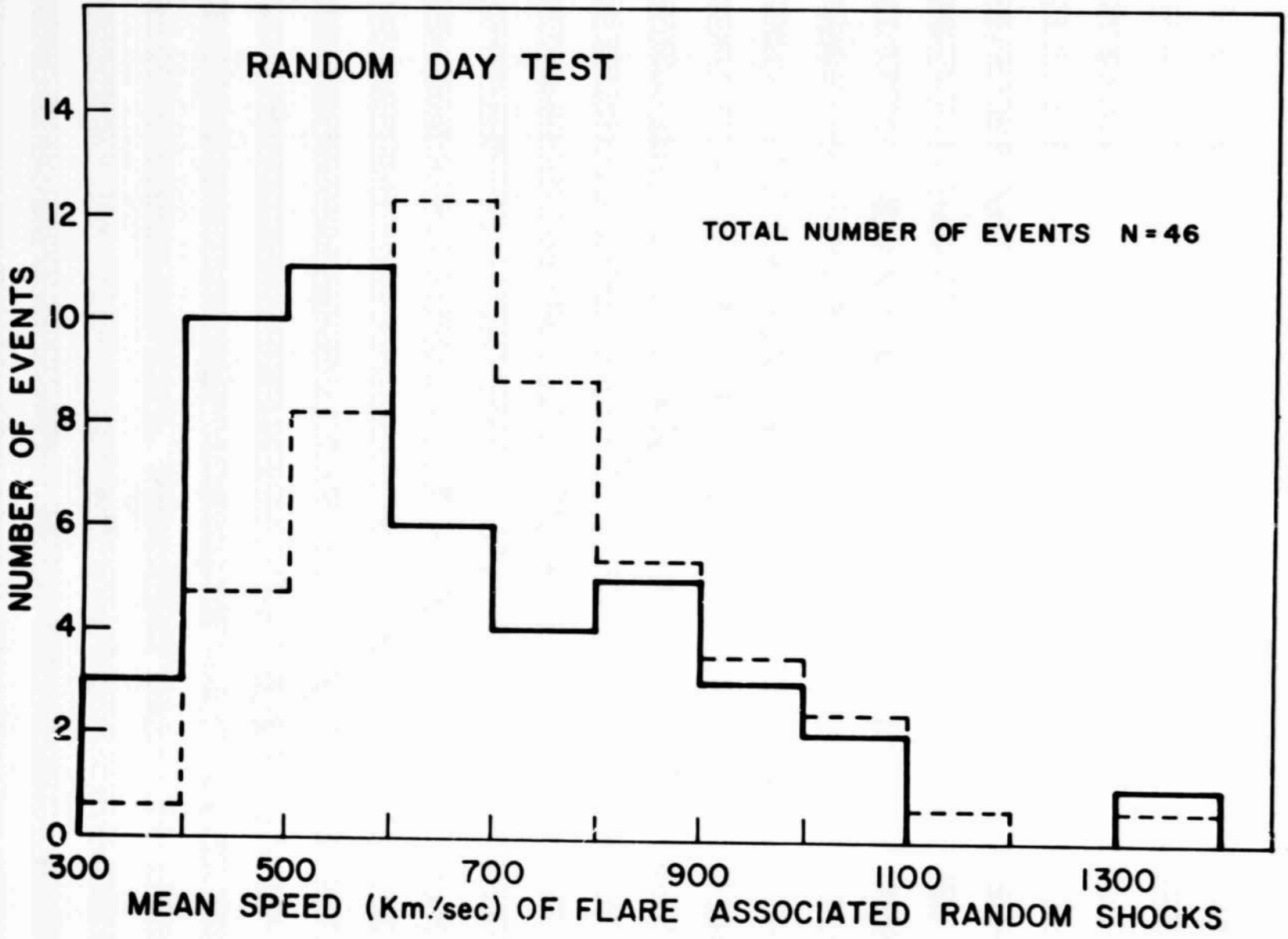
RANDOM DAY TEST
TOTAL NUMBER OF EVENTS N=46
NUMBER OF EVENTS
0
2
4
6
8
10
12
14
300
500
700
900
1100
1300
MEAN SPEED (Km./sec) OF FLARE ASSOCIATED RANDOM SHOCKS

Figure 7

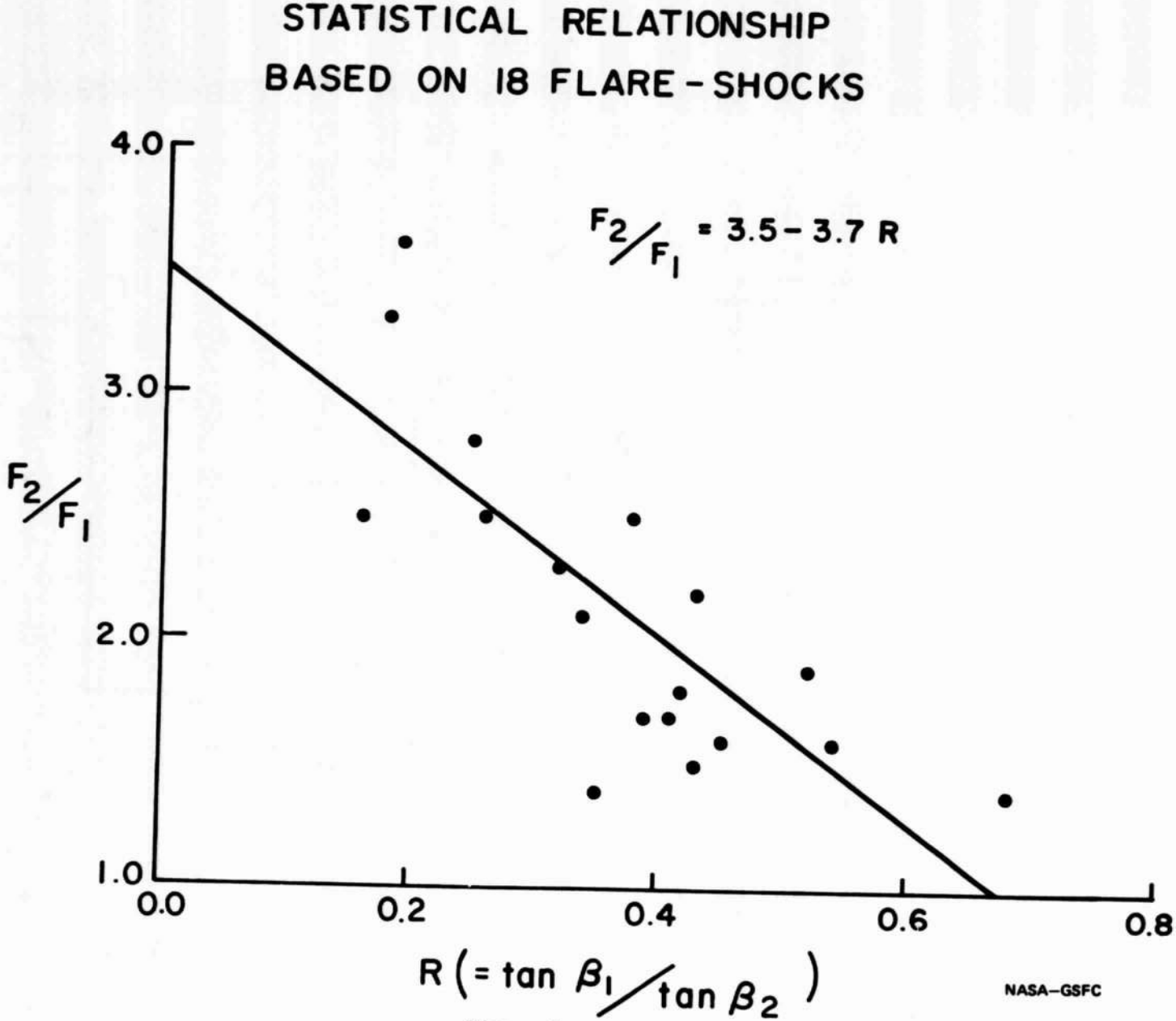
STATISTICAL RELATIONSHIP
BASED ON 18 FLARE-SHOCKS
$F_2/F_1 = 3.5 - 3.7\,R$
4.0
3.0
2.0
1.0
F_2/F_1
0.0
0.2
0.4
0.6
0.8
$R\,(=\tan\beta_1/\tan\beta_2)$
NASA-GSFC

Figure 8